Nanotoxicology, August 2014; 8(5):521–532

ISSN: 1743-5390 print / 1743-5404 online
DOI: 10.3109/17435390.2013.802821

informa
healthcare

Gold-nanobeacons for gene therapy: evaluation of genotoxicity, cell toxicity and proteome profiling analysis

João Conde[1,2], Miguel Larguinho[1,3], Ana Cordeiro[1,3], Luís R. Raposo[4,5], Pedro M. Costa[6], Susana Santos[4,5], Mário S. Diniz[3], Alexandra R. Fernandes[4,5,7], & Pedro V. Baptista[1]

[1]CIGMH, DCV, Faculdade de Ciências e Tecnologia, Universidade Nova de Lisboa, Caparica, Portugal, [2]Instituto de Nanociencia de Aragón, Universidad de Zaragoza, Zaragoza, Spain, [3]REQUIMTE, DQ, Faculdade de Ciências e Tecnologia, Universidade Nova de Lisboa, Caparica, Portugal, [4]Centro de Química Estrutural, Instituto Superior Técnico, Lisboa, Portugal, [5]CB3, FECN, Universidade Lusófona de Humanidades e Tecnologias, Lisboa, Portugal, [6]IMAR, DCEA, Faculdade de Ciências e Tecnologia, Universidade Nova de Lisboa, Caparica, Portugal and [7]DCV, Faculdade de Ciências e Tecnologia, Universidade Nova de Lisboa, Caparica, Portugal

Abstract

Antisense therapy is a powerful tool for post-transcriptional gene silencing suitable for down-regulating target genes associated to disease. Gold nanoparticles have been described as effective intracellular delivery vehicles for antisense oligonucleotides providing increased protection against nucleases and targeting capability via simple surface modification. We constructed an antisense gold-nanobeacon consisting of a stem-looped oligonucleotide double-labelled with 3′-Cy3 and 5′-Thiol-C6 and tested for the effective blocking of gene expression in colorectal cancer cells. Due to the beacon conformation, gene silencing was directly detected as fluorescence increases with hybridisation to target, which can be used to assess the level of silencing. Moreover, this system was extensively evaluated for the genotoxic, cytotoxic and proteomic effects of gold-nanobeacon exposure to cancer cells. The exposure was evaluated by two-dimensional protein electrophoresis followed by mass spectrometry to perform a proteomic profile and 3-(4,5-Dimethylthiazol-2-Yl)-2,5-Diphenyltetrazolium Bromide (MTT) assay, glutathione-S-transferase assay, micronucleus test and comet assay to assess the genotoxicity. This integrated toxicology evaluation showed that the proposed nanotheranostics strategy does not exhibit significant toxicity, which is extremely relevant when translating into *in vivo* systems.

Keywords: antisense, gold nanoparticles, gene silencing, DNA damage, cytotoxicity, proteomics

Introduction

The development of a safe, efficient, specific and non-pathogenic vehicle for gene delivery is highly attractive (Kim et al. 2009; Akhtar & Benter 2007). Nanoparticles (NPs), in particular, are expected to provide a range of devices for diagnosis and treatment in cancer as their dimensions are well matched in size to biologic molecules and structures found inside living cells (Conde et al. 2012b). Gold nanoparticles (AuNPs) have been extensively investigated and applied in conjunction with biomolecules due to their ease of synthesis and functionalisation derived from their large surface-to-volume ratio (Conde et al. 2012a; Doria et al. 2012; Daniel & Astruc 2004; Jain 2008; Haglund et al. 2009). This way, several strategies have been proposed based on AuNPs as intracellular delivery vehicles for antisense oligonucleotides by providing protection against intracellular nucleases and ease of functionalisation for selective targeting (Whitehead et al. 2009; Giljohann et al. 2009; Rana et al. 2012; Ghosh et al. 2008a; Ghosh et al. 2008b; Thomas & Klibanov 2003; McIntosh et al. 2001; Conde et al. 2010; Rosi et al. 2006).

In this study, we used a gold-nanobeacon (Au-nanobeacon) to target and silence a specific mRNA while providing means to assess its effectiveness via fluorescence signalling. The antisense Au-nanobeacon consisting of a stem-looped oligonucleotide double-labelled with 3′-Cy3 and 5′-Thiol-C6 bonded to the AuNPs' surface, whose sequence is capable of blocking enhanced green fluorescent protein (EGFP) expression. This nanoconjugate was tested for the effective blocking of EGFP expression in a colorectal cancer cell-line (HCT-116). The beacon's increase in fluorescence upon hybridisation to the specific target was used to evaluate the effective silencing as a higher level of silencing yields a more intense fluorescence signal from the beacon. Previously, we demonstrated that Au-nanobeacons could successfully be used for assessing the effective level of gene silencing *in vitro* (Rosa et al. 2012; Conde et al. 2013).

Correspondence: Pedro V. Baptista, Department of Life Sciences, Faculdade de Ciências e Tecnologia, Universidade Nova de Lisboa, Campus de Caparica, 2829-516 Caparica, Portugal. Tel: +351212948530. Fax: +351212948530. E-mail: pmvb@fct.unl.pt

(Received 19 February 2013; accepted 2 May 2013)

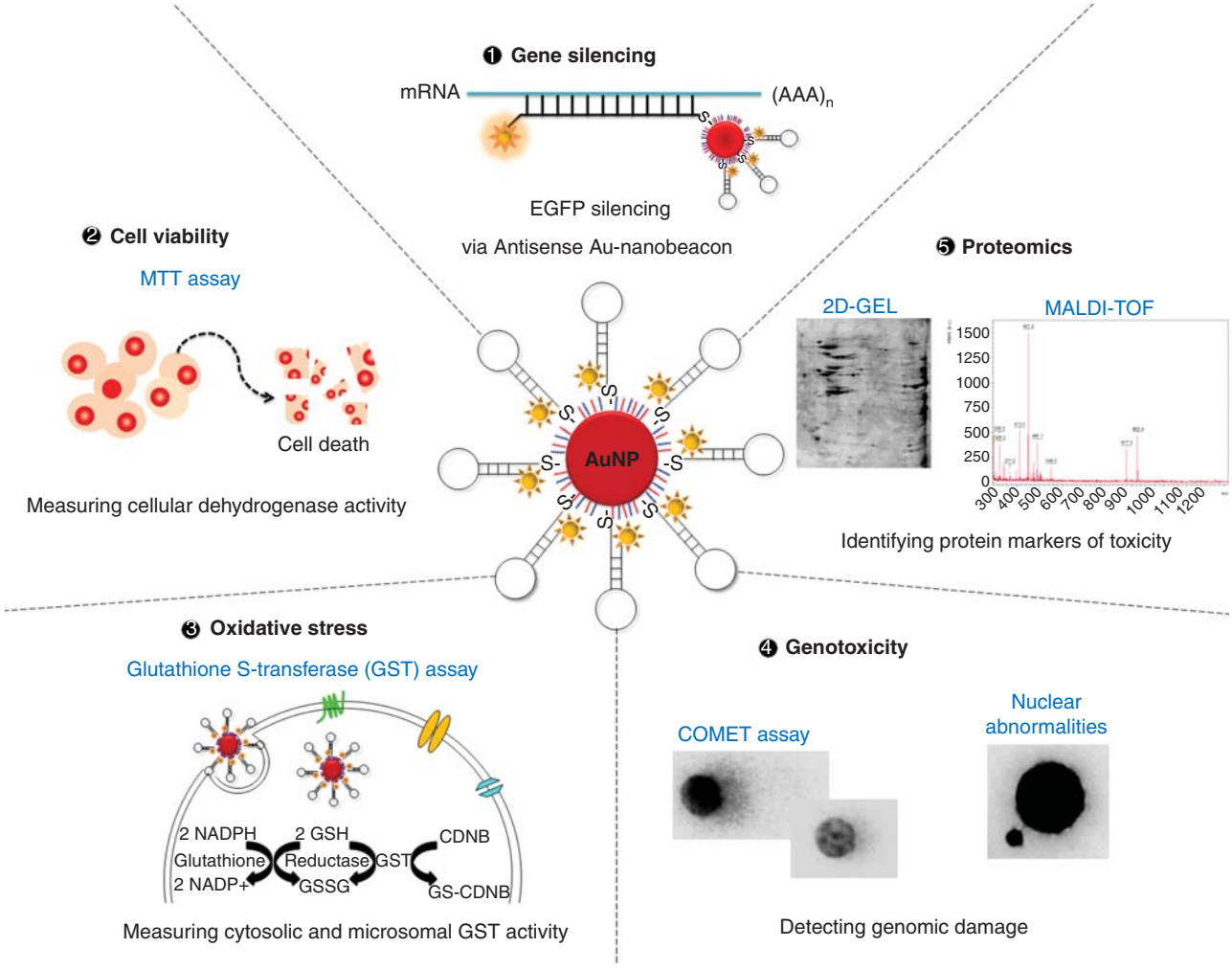

Figure 1. Antisense Au-nanobeacons for gene therapy: from genotoxicity to proteomics. ❶ Gene silencing via antisense Au-nanobeacons; ❷ cell viability (MTT assay); ❸ oxidative stress (glutathione-S-transferase activity); ❹ genotoxicity assessment (NAs and comet assay); and ❺ identifying protein markers by two-dimensional protein electrophoresis followed by peptide mass fingerprinting.

Despite major advances in nanotechnology-based drug delivery, the vast majority of studies merely report on the biocompatibility of nanomaterials relying on cell viability evaluation and cell counting (van et al. 2011; Dobrovolskaia & McNeil 2007; Wall & Shi 2003; Ozpolat et al. 2010). Thus far, little attention has been directed to the detection of genome damage, such as DNA strand breaks and formation of nuclear abnormalities (NAs), characterisation of protein markers of toxicity or measuring the level of oxidative stress. When considering the toxicity of AuNPs, size, concentration and surface coating also play a role in triggering cellular and physiologic response (Alkilany & Murphy 2010). For instance, poly(ethylene glycol) (PEG)-coated AuNPs have been shown to exhibit size-dependent *in vivo* toxicity and PEG alone is known to trigger cellular stress (Zhang et al. 2011). All these markers are of great importance when assessing biocompatibility and safety of the nanomaterials if they are to be used for medical purposes, and ought to be used as primary screen once therapeutic effect is demonstrated (Dobrovolskaia & McNeil 2007). Identification of these disease/toxicity biomarkers may allow improvement of safety assessment of nanomaterials.

Here, following demonstration of the Au-nanobeacons' gene silencing capability, the system was extensively evaluated in terms of cellular toxicity, namely at the proteomic and genomic level. HCT-116 cells were exposed to antisense Au-nanobeacons as putative nanotheranostics tool, and toxicity evaluated using MTT assay, glutathione-S-transferase assay, NAs and comet assay, and two-dimensional protein electrophoresis followed by mass spectrometry for identification of putative stress markers (see Figure 1).

Methods

Synthesis of citrate-AuNPs

AuNPs were synthesised by the citrate reduction method described by Lee and Meisel (1982). Citrate-capped AuNPs were characterised by transmission electron microscopy (TEM) and UV-Vis spectroscopy (seeSupplementary Figure S1A-B).

Synthesis of PEGylated-gold nanoparticles

Functionalisation of PEGylated AuNPs was carried out using commercial hetero-functional PEG functionalised with a thiol group O-(2-Mercaptoethyl)-O′-methyl-hexa(ethylene glycol), $C_{15}H_{32}O_7S$, 356.48 Da (Sigma), as previously

described (Rosa et al. 2012; Conde et al. 2013; Sanz et al. 2012). Excess PEG was removed by centrifugation (21.460 × *g*, 30 min, 4°C), and quantified by the Ellman's Assay suitable for sulfhydryl group determination.

Synthesis of gold nanobeacons (AuNP@PEG@Beacon)

The antisense Au-nanobeacon contains a stem-looped oligonucleotide double-labelled with 3′-Cy3 and 5′-Thiol-C6(5′-TTTGCCTCGTCGCTCTCCATGGTGGGCAAA-3′)complementary to the Kozak consensus translation initiation site and start codon of the EGFP (pVisionGFP-N vector 4.7 kb, Biovision), thus capable of blocking the translational machinery. The nonsense Au-Nanobeacon contains a stem-looped oligonucleotide of unrelated sequence double-labelled with 3′-Cy3 and 5′-Thiol-C6 (5′-TTTGCC CCGTTACTATTTGCACCACGGCAAA-3′). Briefly, the thiolated oligonucleotides (STABVIDA) were suspended in 1 mL of 0.1 M dithiothreitol (DTT), extracted three times with ethyl acetate and further purified through a desalting NAP-5 column (Pharmacia) using 10 mM phosphate buffer (pH 8) as eluent. Following oligonucleotide quantification via UV/Vis spectroscopy, each oligomer was added to the AuNP@PEG solution in a 100:1 ratio. AGE I solution [2% (w/v) sodium dodecyl sulphate (SDS), 10 mM phosphate buffer (pH 8)] was added to the mixture to achieve a final concentration of 10 mM phosphate buffer (pH 8), 0.01% (w/v) SDS. The solution was sonicated for 10 sec using an ultrasound bath and incubated at room temperature for 20 min. Afterwards, the ionic strength of the solution was increased sequentially in 50 mM NaCl increments by adding the required volume of AGE II solution (1.5 M NaCl, 0.01% (w/v) SDS, 10 mM phosphate buffer (pH 8)) up to a final concentration of 10 mM phosphate buffer (pH 8), 0.3 M NaCl, 0.01% (w/v) SDS. After each increment, the solution was sonicated for 10 sec and incubated at room temperature for 20 min before the next increment. Following the last addition, the solution was left to rest for additional 16 h at room temperature. Then, the functionalised Au-nanobeacons were centrifuged for 20 min at 21.460 × *g*, the oily precipitate washed three times with Diethyl Pyrocarbonate (DEPC)-treated H_2O, and redispersed in the same buffer to a final concentration in Au-nanobeacons of 15 nM. The resulting Au-nanobeacons were stored in the dark at 4°C until further use. Au-nanobeacons were characterised by dynamic light scattering (DLS) (Zetasizer, Malvern), Zeta Potential (Zetasizer, Malvern), UV/Vis Spectroscopy and TEM (see Supplementary Figure S1C–F).

Quantitation of beacon coverage on AuNP@PEG

Coverage, i.e. average number of labelled beacons per NP was assessed by quantification of the thiolated oligonucleotides in supernatant from the Au-nanobeacon synthesis. All the three supernatants containing the unbound oligonucleotides were measured by monitoring the emission spectra of Cy3 (Exc = 530 nm) dye in a Cary Eclipse (Varian) using an Ultra-Micro quartz cell (Hëllma). All AuNP samples and standard solutions of the thiol-oligonucleotide beacon were kept at the same pH and ionic strength and calibration for all measurements. Fluorescence emission was converted to molar concentrations by interpolation from a standard linear calibration curve, prepared using the same buffer pH and salt concentrations.

Cell culture and EGFP vector transfection

As a model system, HCT-116 cells (from colorectal carcinoma) were grown in Dulbecco's modified Eagle's medium with Glutamax (DMEM, Invitrogen) with 10% heat-inactivated fetal bovine serum (Invitrogen), 100 U/mL penicillin and 100 μg/mL streptomycin (Invitrogen), and maintained at 37°C in 5% CO_2. Cells were seeded at a density of 1×10^5 cells/well in 24-well plates and grown for 24 h prior to transfection of EGFP vector (pVisionGFP-N vector 4.7 kb, Biovision) encoding green fluorescent protein optimised for high expression in mammalian cells. On the day of transfection, cells were approximately 50% confluent. EGFP vector (1 μg per well) was added with 2 μg of Lipofectamine 2000® (Invitrogen) and Opti-MEM® Reduced Serum Medium (Invitrogen) according to the manufacturer's recommendations (see Supplementary Information S2).

EGFP silencing with antisense Au-nanobeacon

After 24 h of EGFP transfection, cells were treated with 30 nM of antisense Au-nanobeacons in Opti-MEM® reduced serum medium (Invitrogen). After 48 h, cells were washed with 1× PBS, lysed in ultrapure water and collected for analysis of EGFP silencing, RNA extraction and confocal imaging. Fluorescence was measured at least three times in a Cary Eclipse spectrofluorimeter (Varian) using an Ultra-Micro quartz cell (Hëllma) by taking the area under the curve from 495 to 650 nm. EGFP fluorescence values were normalised to the bulk protein concentration determined via the Bradford assay (Thermo Scientific), and then normalised against the controls to determine percent knockdown of EGFP.

qRT-PCR

Total RNA was extracted from the cell line using the Trisure reagent (Bioline) according to the manufacturer's protocol, and used for quantitative real-time polymerase chain reaction (qRT-PCR) to evaluate expressions of EGFP and β-actin. cDNA was obtained by subjecting 1 μg of total RNA to reverse transcription with 200 U of Revert-AidTM M-MuLV reverse transcriptase (Fermentas) according to the manufacturer's specifications, using 20 μM of EGFP and β-actin reverse primers, annealing at 42°C for 1 h and 70°C for 10 min for reverse transcriptase inactivation. Real-time PCR amplification was performed in a Corbett Research Rotor-Gene RG3000 using SYBR GreenER real-time PCR kit (Invitrogen) according to the manufacturer's specifications in 50 μL reactions containing 2 μl of cDNA, 1× SYBR Green SuperMix and 200 nM of primers (STABVIDA). The following primers were employed: β-actin forward 5′-ATAGCACAGCCTGGATAGCAAC-3′; β-actin reverse 5′-CACC TTCTACAATGAGCTGCGT-3′; EGFP forward 5′-AGCTTCG AATTCTGCAGTCG-3′; EGFP reverse 5′-GGCTGATTATGAT CTAGAGTC-3′. The amplification conditions consisted of 50°C for 2 min hold, 95°C during 10 min hold, followed by 40 cycles consisting of denaturation at 95°C for 30 sec,

annealing at 52°C for 60 sec, extension at 72°C for 45 sec, with a final extension step at 72°C for 10 min. All the results were originated from three independent experiments. Threshold cycle values were analysed by the ΔCt method (Livak & Schmittgen 2001; Pfaffl 2001), once the difference of PCR amplification efficiency of EGFP and β-actin products was less than 5% (Efficiency = $10^{(-1/\text{slope})} - 1$). The β-actin expression levels were used as reference, and fold-induction was calculated by the Ct method as follows: $\Delta CT = (Ct\ EGFP - Ct\ \beta\text{-actin})_{\text{treated for EGFP}} - (Ct\ EGFP - Ct\ \beta\text{-actin})_{\text{untreated}}$. The final data were then derived from $2^{-\Delta CT}$. The expected sizes of the PCR products were 158 bp (β-actin) and 792 bp (EGFP). The PCR products were subjected to electrophoresis on a 2% agarose gel (TBE 1×), during 75 min at 90 V, stained with GelRed (Biotium) and visualised under UV light.

Confocal microscopy

HCT-116 cells were seeded at a concentration of 1×10^5 cells/well in 24-well plates on glass slides in 500 μL of DMEM (Invitrogen) with 10% heat-inactivated fetal bovine serum (Invitrogen) and maintained at 37°C in 5% CO_2. All confocal microscopy samples were prepared under the same conditions as described above for GFP silencing and recovery. Cells were fixed with 4% paraformaldehyde in PBS for 15 min at 37°C and mounted in ProLong® Gold Antifade Reagent with DAPI (Invitrogen) to allow for nuclear staining. Images were acquired with a confocal laser point-scanning microscope Zeiss LSM 510 META, with excitation at 405 nm for DAPI (nucleus), 480 nm for EGFP and 561 nm for Cy3 (Au-nanobeacons).

MTT assay

Standard MTT [3-(4,5-dimethylthiazol-2-yl)-2,5-diphenyltetrazoliumbromide] reduction assay (Invitrogen) was performed to determine the cytotoxicity of the functionalised AuNP complexes. Briefly, cells were seeded at a density of 1×10^5 cells per well in 24-well culture plates in complete DMEM (500 μl) with serum. After 24 h, 100 μl of functionalised AuNPs under the same conditions of the EGFP knockdown/recovery experiments were added and cells further incubated for 48 and 72 h. The medium was then removed and cells were washed twice with sterile PBS and 300 μl of fresh medium with serum was added. For the assay, 16.7 μl of sterile MTT stock solution (5 mg/mL in PBS) were added to each well, incubated for 2 h, the medium removed and the formazan crystals resuspended in 300 μl of dimethyl sulphoxide (DMSO) (Sigma). The solution was mixed and its absorbance was measured at 540 nm as working wavelength and 630 nm as reference, using a Microplate reader Infinite M200 with an absorbance module (Tecan). The cell viability was normalised to that of cells cultured in the culture medium with PBS treatment. The experiments were repeated three times.

Genotoxicity assessment

Genotoxic effects were assessed by quantification of DNA strand breakage, through the alkaline version of comet assay (Costa et al. 2008; Singh et al. 1988) and frequency of NAs. Forty-eight hours after treatment with the Au-nanobeacons (with or without Lipofectamine), HCT-116 cells were centrifuged and the pellet resuspended in 50 μL of 1× PBS. From this suspension, a drop containing approximately 2.5×10^5 cells was smeared on glass microscope slides and left to dry at room temperature for subsequent analysis of NAs. Preparations were methanol-fixed (for 15 min), stained with 0.1 g/L acridine orange and mounted using the non-fluorescent DPX resin (from BDH) (Costa & Costa 2007). The frequency of cells with NAs was determined by scoring 1000 cells per preparation, following criteria established elsewhere (Fenech et al. 2003) (see Supplementary Information S3). For the comet assay, glass microscope slides were previously coated with 1% (w/v) agarose (normal melting point) in 1× TAE buffer and left to dry for at least 48 h, at 37°C. Sample preparation was as follows: 2 μL of the cell suspension in 1× PBS was diluted in 310 μL of 1% (w/v) liquid low melting-point agarose (LMPA) in 1× PBS (35–40°C). One hundred and fifty microlitres of cell-containing LMPA were spotted onto the prepared glass slides (1.1×10^4 cells per slide) and covered with a coverslip. Upon agarose solidification, coverslips were removed and the slides dipped into lysis solution (450 mM NaCl; 3.72% EDTA; 5 mM TRIS; to which 10% (v/v) DMSO and 1% (v/v) Triton-X were added just before use) during 1 h at 4°C, followed by 40 min into cold electrophoresis solution (1 mM EDTA; 300 mM NaOH, pH 13) to ensure DNA unwinding and promote expression of alkali-labile sites. Electrophoresis was carried out at 4°C, for 30 min, at 25 V using a Sub-Cell model 96 apparatus (Bio-Rad). Afterwards, slides were placed into 0.1 M Tris–HCl buffer (pH 7.5) during 15 min for neutralisation. All described steps were performed under strictly controlled temperature and light conditions to minimise accessory DNA degradation and gel lifting from slides. Upon staining with ethidium bromide (20 μg/mL), an approximated number of 100 intact nucleoids per slide was analysed, using the CometScore software v.1.5 (TriTek Corp.). The DNA percentage in the comets' tail was employed as metrics for total DNA strand breakage. Both imaging analyses were performed by epifluorescence microscopy, on a DLMB microscope equipped with an EL6000 light source (Leica Microsystems), using an I3 filter (for acridine orange staining) and N2.1 filter (for ethidium bromide staining).

Measurement of glutathione-S-transferase activity

After the 48-h treatment, cells were washed with 1× PBS, lysed in ultrapure water and the pellets resuspended in 50 μL ultrapure water. Briefly, glutathione s-transferase (GST) activity was determined based on a procedure described by Habig et al. (1974) by measuring the conjugation of 1-chloro-2,4-dinitro benzene with glutathione (GSH). The enzyme activity was determined by measuring the absorbance at every minute during a maximum of 10 min on a 96-well plate (SPL LifeSciences), using 3 replicas for each sample. The change in absorbance was measured at 340 nm using an Infinite 2000 Microplate reader (Tecan) and values were normalised to total protein concentration determined by the Bradford assay (Thermo Scientific).

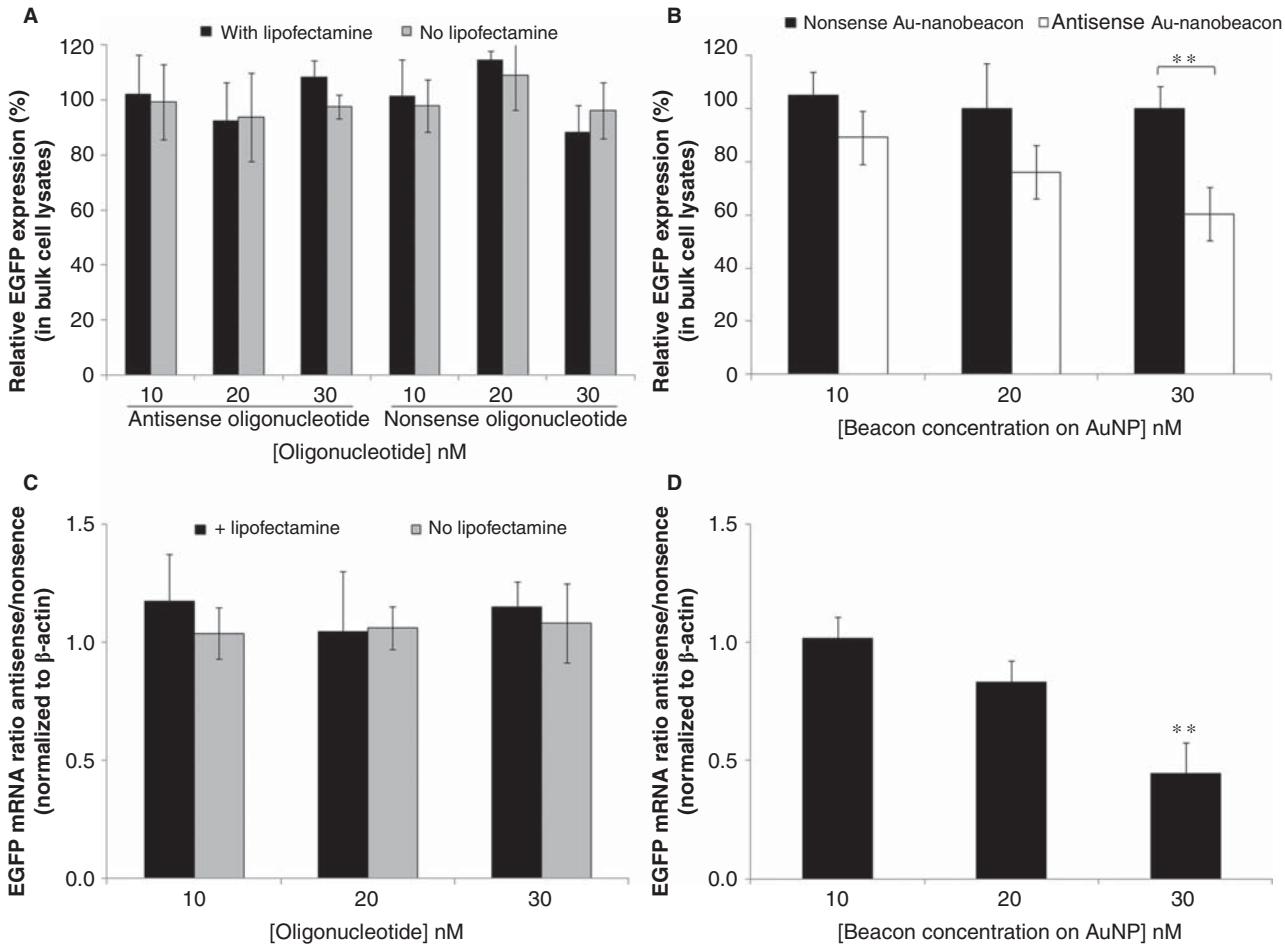

Figure 2. Quantitative assessment of EGFP silencing efficiency via antisense Au-nanobeacons, nonsense Au-nanobeacon and naked oligonucleotides. (A,B) EGFP silencing was confirmed by measurement of EGFP intensity in bulk cell lysates (as percentage of original EGFP fluorescence levels) using an antisense and a nonsense oligonucleotide (without AuNP) (A) and with antisense and nonsense Au-nanobeacons (B). EGFP silencing was confirmed by significant fluorescence decrease when compared to non-treated cells (**, $p \leq 0.005$) in bulk cell lysates at 30 nM of antisense Au-nanobeacon only. EGFR mRNA expression confirmed by qRT-PCR for antisense and nonsense oligonucleotides (C); and with antisense and nonsense Au-nanobeacons (D), using β-actin as reference.

Protein sample preparation

To minimise sample degradation, all solutions for sample preparation contained 1× phosphatase inhibitor (PhosStop, Roche), 1× protease inhibitor (cOmplete Mini, Roche®), 1 mM PMSF and 0.1% (w/v) DTT. After treatment, cells were collected and concentrated in lysis buffer (150 mM NaCl; 50 mM Tris, pH = 8.0; 5 mM EDTA, 2% (w/v) NP-40) by centrifugation at 14,000 × *g* for 30 min at 4°C. Supernatant was collected and samples stored at −80°C.

Two-dimensional gel electrophoresis

Prior to two-dimensional gel electrophoresis, protein concentration was determined via the 2-D Quant kit (GE Healthcare). Isoelectric focusing was performed using immobilised pH gradient strips (GE Healthcare) in an Ettan-nIPGphor 3 focusing unit (GE Healthcare) according to Teixeira et al. (2005) (see Supplementary Information S4). Variation of each protein expression level was calculated as the ratio of the normalised intensity of each protein spot in gels corresponding to each condition compared to those corresponding to control samples. The Mr values for the identified proteins were determined by comparison with the relative positions of the proteins included in the molecular weight protein marker (HyperPAGE, Bioline), which were run for the second dimension with the samples under study. Spots with significantly altered intensities between conditions (up- or down-regulated proteins in comparison to control samples) were selected and picked from gels towards identification via matrix-assisted laser desorption/ionisation-time of flight mass spectrometry.

Statistical analysis

All statistical analyses were performed with SPSS statistical package (version 15, SPSS Inc., Chicago, IL, USA). Data derived from the comet assay, frequencies of cells with NAs and GST activity were analysed using non-parametric statistics, namely the Mann–Whitney *U* tests for pairwise comparisons between experimental conditions. A statistical significance threshold $\alpha = 0.05$ was set for all analyses.

Results

Synthesis and characterisation of Au-nanobeacons

The synthesised citrate-capped AuNPs were characterised by: TEM, showing an average diameter of 14.6 ± 1.7 nm, in good agreement with DLS measurement (average diameter

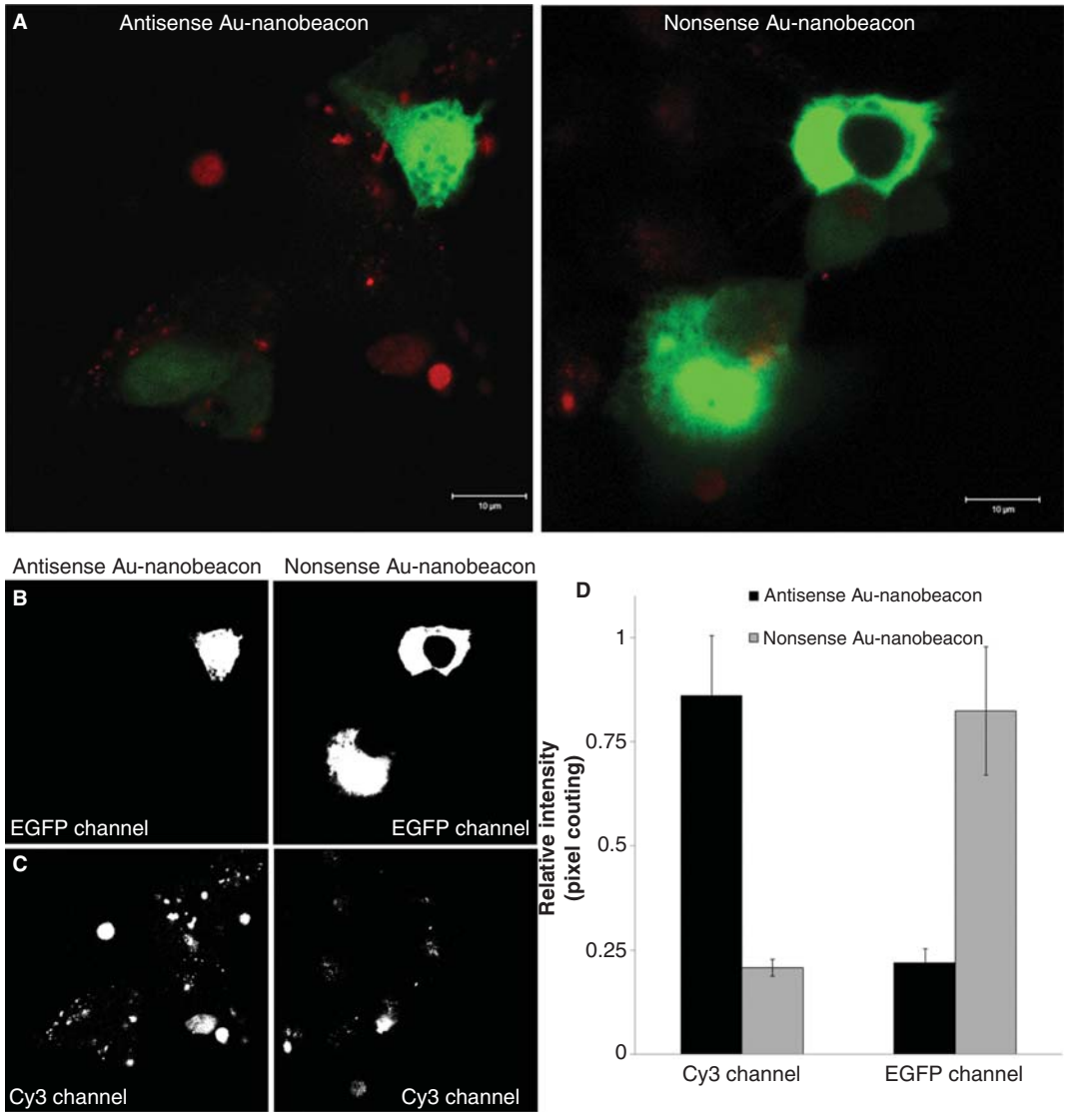

Figure 3. Confocal fluorescence imaging of antisense and nonsense Au-nanobeacons effect in HCT-116 cells. Confocal imaging (scale bar, 10 μm) shows HCT-116 cells expressing EGFP after exposure to 30 nM of antisense and nonsense Au-nanobeacons (A). EGFP expression levels can be evaluated by the intensity of its fluorescence (green, EGFP) (B) and Au-nanobeacons in open conformation (red, Cy3) can be identified as fine punctuation dispersed throughout the cytoplasm (C). Relative fluorescence intensity of Cy3 and EGFP channels for antisense (black bars) and nonsense (grey bars) Au-nanobeacons obtained after individual colour channel analysis of the same confocal images using ImageJ software (D).

of 16.7 ± 5.9 nm) with a relatively narrow distribution with a polydispersity index of 0.294 ± 0.017; a Zeta potential of −28.6 ± 2.4 mV at pH 7; and the characteristic surface plasmon resonant peak at 519 nm (Supplementary Figure S1). These AuNPs were then functionalised with a PEG spacer to increase stability, biocompatibility and grant chemical functionality as well as avoid opsonisation (Liu et al. 2007). The PEGylated AuNPs (AuNP@PEG) showed a 30% saturated PEG layer (190.29 ± 19.56 PEG chains per NP), which allows the incorporation of the thiolated fluorescence-labelled hairpin oligonucleotide capable of blocking the transcriptional machinery – *antisense Au-nanobeacon* (57.87 ± 3.92 hairpins per NP); or an unrelated stem-looped oligonucleotide – *nonsense Au-nanobeacon* (31.64 ± 3.49 hairpins per NP). The determination of the degree of saturation of AuNPs functionalised with thiolated PEG chains and quantification of molecular beacon strands per NP was extensively discussed elsewhere (Rosa et al. 2012; Conde et al. 2013).

Au-nanobeacon for gene silencing – a nanotheranostics tool

EGFP knockdown studies were conducted in colorectal cancer cells (HCT-116 cells) using an EGFP expression plasmid as a target model. Quantification of EGFP expression by direct measurement of EGFP fluorescence levels (Figure 2A and B) reveals that only the antisense Au-nanobeacon at 30 nM down-regulates EGFP expression (Figure 2B). The use of Lipofectamine did not result in EGFP silencing (Figure 2A). These data are corroborated by qRT-PCR (Figure 2C and D). A significant fluorescence decrease (55.57 ± 13.34% EGFP down-regulation) was observed at 30 nM of antisense Au-nanobeacon (Figure 2D).

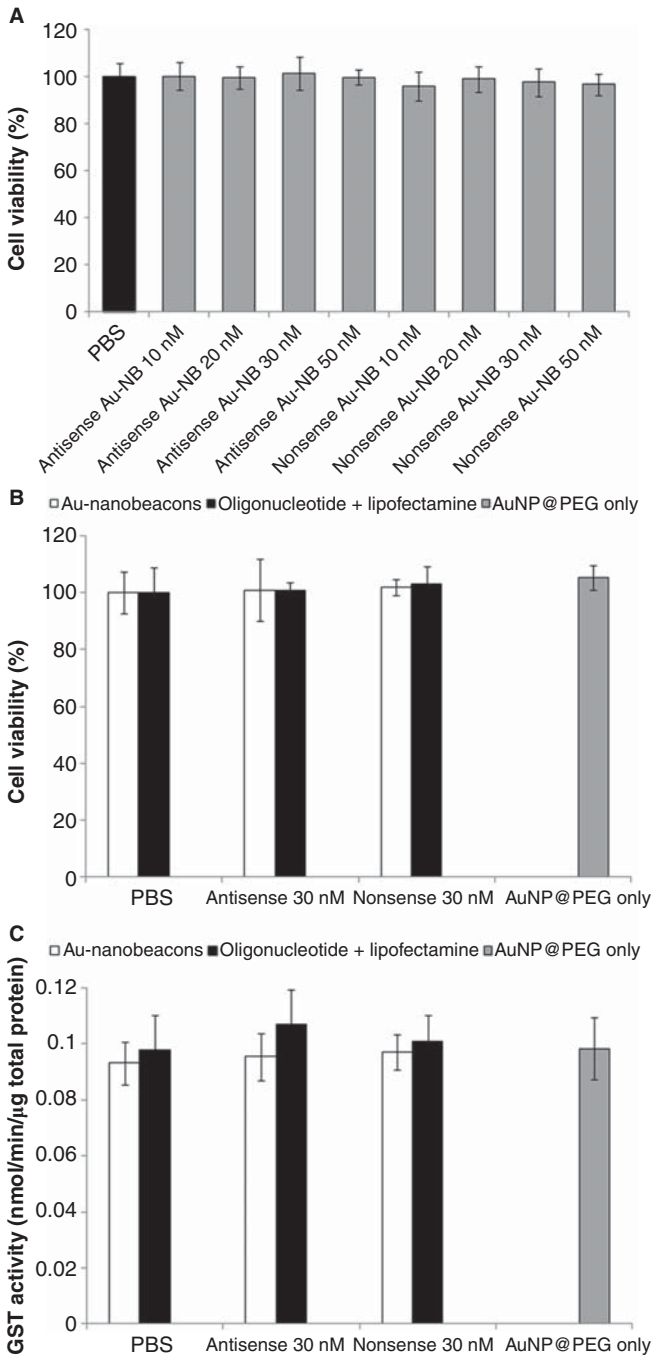

Figure 4. MTT and GST assays in human colorectal cancer cells (HCT-116). (A) Cell viability (MTT assay) with increasing concentrations of the nanoformulations used in this study. Negligible influence is observed for all concentrations tested when compared to untreated cells (black bar). (B) MTT assay for all (nano)biomolecular assemblies (30 nM) administered in the present study at 48 h of exposure. Negligible influence in cell viability is observed for all assemblies tested when compared to untreated cells (PBS). (C) GST activity was measured for both antisense and nonsense Au-nanobeacons and naked oligonucleotides at 30 nM.

Confocal fluorescence imaging shows that cells that internalised the antisense Au-nanobeacon exhibit lower fluorescence compared to those treated with nonsense Au-nanobeacon (Figure 3A). Moreover, cellular distribution of the Au-nanobeacon is observed by the punctuate fluorescence pattern. Data from the Cy3 channel show that antisense Au-nanobeacon leads to higher signal intensity than that of the nonsense Au-nanobeacon (Figure 3B and C). Striking differences for Cy3 and EGFP emissions related to the antisense and nonsense Au-nanobeacon effect can be observed in Figure 3D.

Toxicity assessment of Au-nanobeacons

To characterise the system effects in terms of cell viability, metabolic stress and DNA damage (genotoxicity) and evaluate the potential of the antisense Au-nanobeacon as nanotheranostics tool, we assessed acute toxicity parameters for all tested conditions: cell survival rates (MTT assay), oxidative stress (glutathione-S-transferase assay) and genomic DNA damages (comet assay and frequency of NAs). Regarding the MTT assay, which determines mitochondrial activity in living cells, no cell viability changes were detected up to 48 h incubation for both antisense and nonsense Au-nanobeacons (Figure 4A) and oligonucleotides only at 30 nM (Figure 4B). No major changes in GST activity, which is often used as an oxidative stress biomarker, were observed for antisense and nonsense Au-nanobeacons or for the naked oligonucleotides (Figure 4C) and no significant differences were observed amongst all samples ($p < 0.05$).

Genotoxicity was assessed in cells treated with nanobeacon/oligonucleotide concentrations of 30 nM using two standard techniques: single-cell gel electrophoresis (comet assay) and frequency of NAs. According to the % of DNA in tail, comets were assigned to one of five different classes (0–4, corresponding to <20%, 20–40%, 40–60%, 60–80% and >80% total DNA strand breakage). Reference images for the different classes of comets are shown in Figure 5A. Cells from the control treatment (i.e. cells expressing EGFP) exhibited an average of 46.58 ± 10.36% DNA in tail, similar to that observed in cells treated with AuNP@PEG (45.70 ± 12.58%). Cells treated with antisense (39.66 ± 3.84%) and nonsense (32.28 ± 5.13%) Au-nanobeacons failed to yield any significant differences to that of controls ($p < 0.05$). Additionally, the nucleoid distribution per class is uniform amongst these samples as minor or no alterations are observed (Figure 5B). Significant differences ($p < 0.05$) arise, however, in cells transfected with Lipofectamine and both antisense (23.09 ± 1.63%) or nonsense (25.26 ± 8.15%) oligonucleotides, when compared with the treatment with Lipofectamine alone (43.93 ± 5.05%). Similarly, differences in class distribution are denoted (Figure 5B). Despite these differences, treatment with Lipofectamine alone does not differ significantly from the control experiment. Comparing antisense with nonsense oligonucleotide treatments (Figure 5C), no significant differences were found between Au-nanobeacons or Lipofectamine use for internalisation. DNA tail percentages above 80% have not been observed with our approach. Regarding the NA frequency, different abnormalities, such as micronuclei or nuclear buds, were surveyed to determine the average frequency of abnormalities for each treatment – see Figure 5J (for reference, different scored abnormalities are included in Figure 5D–I). The most frequently observed NAs were micronuclei (>95%). Data show no significant differences between samples ($p < 0.05$): cells expressing EGFP show a frequency of 2.60 ± 1.14%, similar to those treated with AuNP@PEG

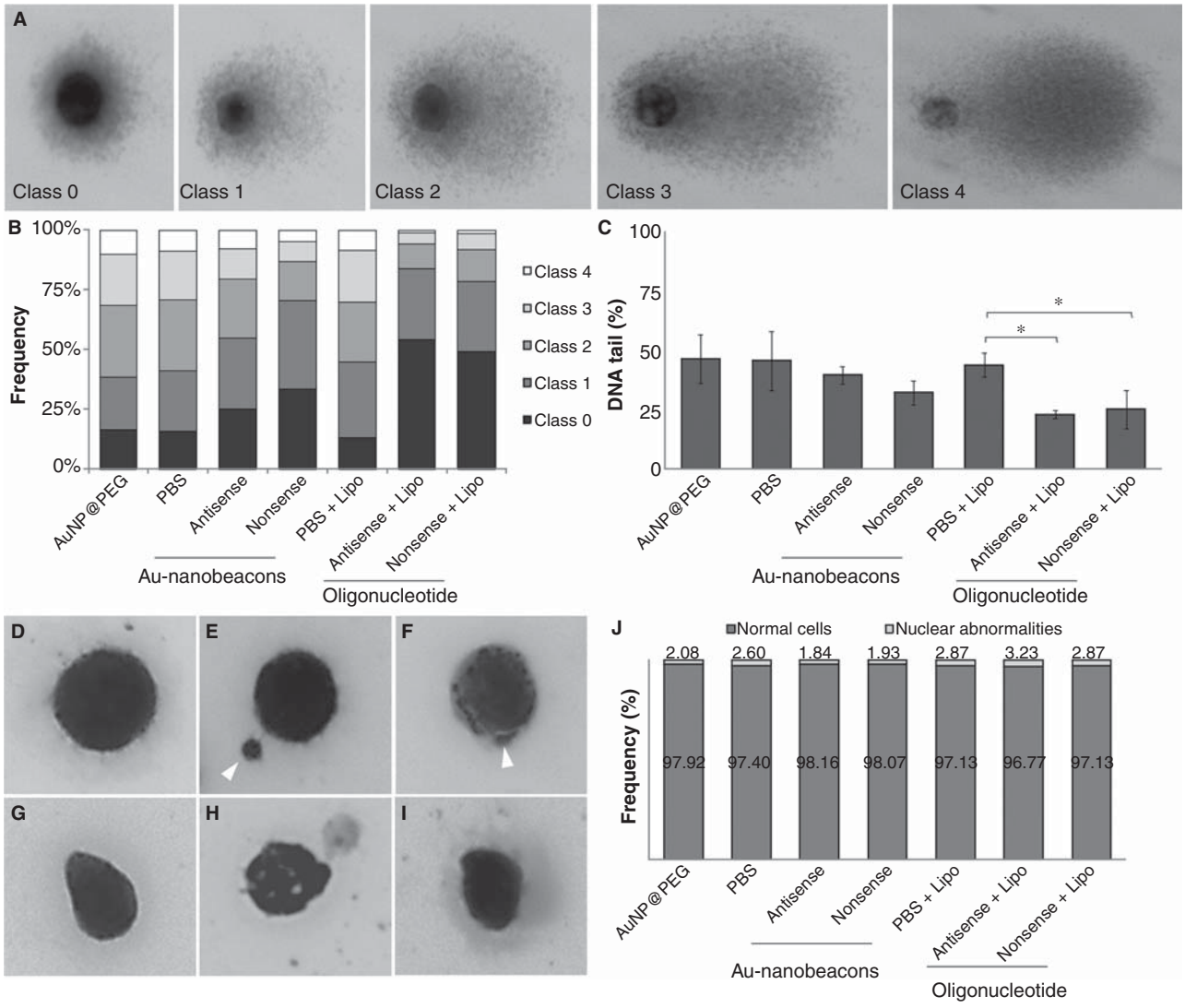

Figure 5. Comet assay and NA frequency for evaluation of genotoxic effects in human colorectal cancer cells (HCT-116). (A) Fluorescent microscopy images of comet classification according to DNA % in tail: class 0 (0–20%); class 1 (20–40%); class 2 (40–60%); class 3 (60–80%); class 4 (80–100%). (B) Relative frequency profile of comet class distribution according to DNA % in tail. (C) Average DNA % in tail assessed for each treatment. (D–I) Fluorescent microscopy reference images of observed NAs: D (normal nucleus); E (single micronucleus, highlighted with an arrow); F (nuclear bud, highlighted with an arrow); G–I (irregular shaped nuclei exhibiting nuclear lobes and buds). (J) NA frequency analysis. Significant differences ($p < 0.05$) marked with *.

(2.08 ± 0.64%), and cells transfected with either the antisense (1.84 ± 0.69%) or the nonsense (1.93 ± 1.10%) Au-nanobeacon. Average frequency of cells transfected with and without Lipofectamine is equivalent ($p < 0.05$).

Proteome profiling

To have additional insights into the cellular toxicity of Au-nanobeacons, colorectal cancer cells (HCT-116) previously transfected with EGFP were used for proteome profiling. Firstly, the effect of Lipofectamine (transfection vehicle; PBS+Lipo) or AuNPs (as vectors for gene silencing; AuNP@PEG) in the proteome of HCT-116 cells was evaluated. A total of five proteins (T-complex protein 1 subunit alpha, 40S ribosomal protein SA and alpha-enolase in Figure 6A-PBS +Lipo and Ezrin and 40S ribosomal protein SA in Figure 6A-AuNP@PEG; Supplementary Figure S4B-C and Table S1) show an increased expression (more than threefold) when compared to control (Figure 6A-PBS; Supplementary Figure S4A; Table S1). Protein 40S ribosomal protein SA was overexpressed (8-fold and 18-fold) in PBS+Lipo and AuNP@PEG, respectively (Figure 6A; Supplementary Figure S4B-C and Table S1). In the presence of Lipofectamine, 19 additional proteins were identified with less than 2-fold overexpression, most of them acting as molecular chaperones that assist protein folding (Figure 6A; Supplementary Figure S3B-C and Table S1). The exposure of EGFP transfected colorectal cancer cells to naked antisense or nonsense oligonucleotides revealed no major toxicity when compared with EGFP transfected cells (PBS+Lipo) (Figure 6A, Supplementary Figure S4-D-E and Table S1). Interestingly, protein 40S ribosomal protein SA and alpha-enolase, which were up-activated in control cells, have an almost normal level of expression in the presence of both oligonucleotides. Also, actin cytoplasmatic 2 was slightly activated (twofold) (Figure 6A, Supplementary Figure S4-D-E and Table S1).

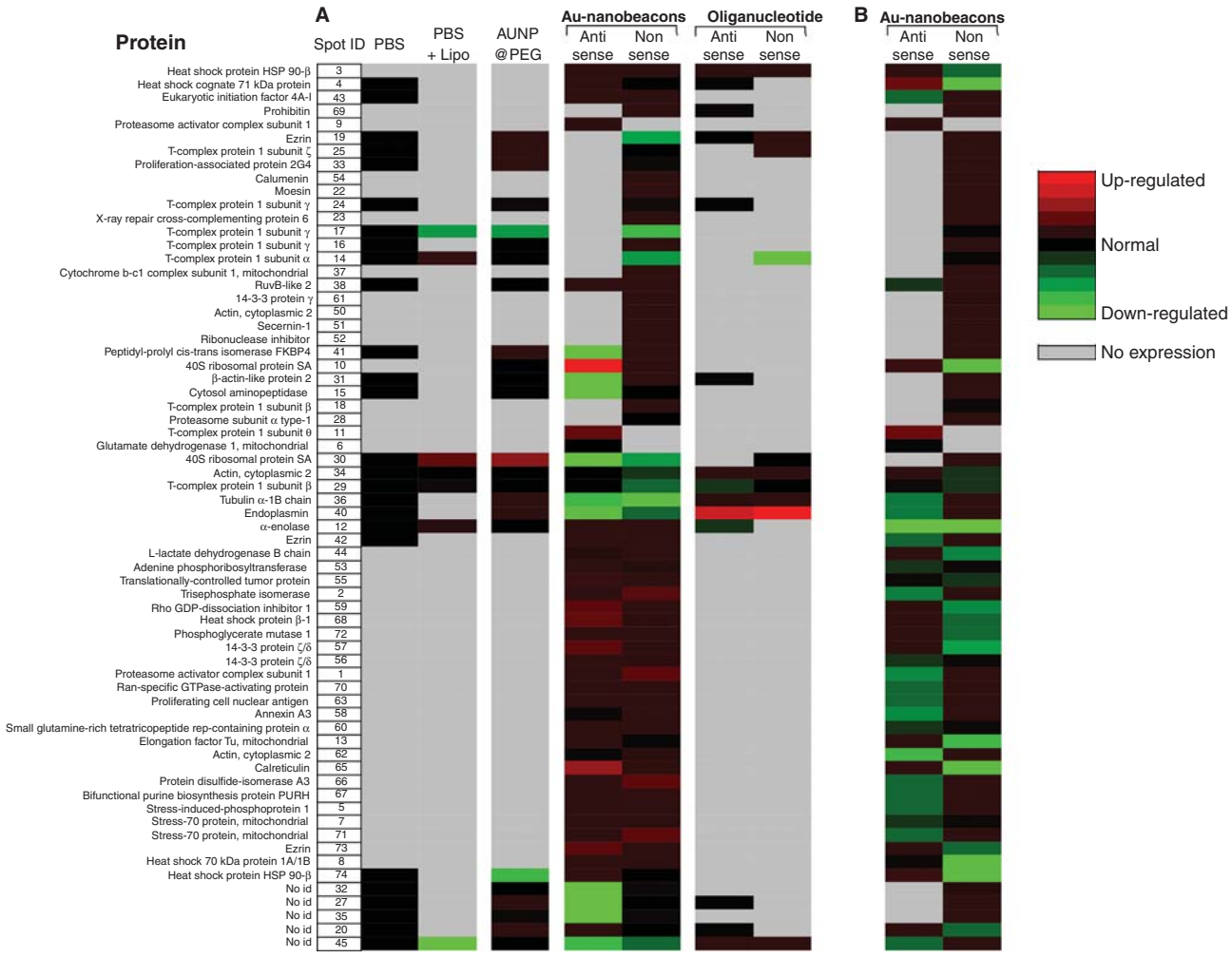

Figure 6. Proteome profiling – comparative levels of protein expression in HCT-116 cells previously transfected with EGFP. Incubated with (A) PBS, PBS + Lipofectamine (PBS + Lipo), AuNPs (AuNP@PEG), antisense Au-nanobeacon, nonsense Au-nanobeacon, naked antisense oligonucleotide, naked nonsense oligonucleotide; and (B) ratios of antisense Au-nanobeacon/nonsense Au-nanobeacon and nonsense Au-nanobeacon/antisense Au-nanobeacon.

To enquire the cellular toxicity of antisense and nonsense Au-nanobeacons, protein expression levels in EGFP-transfected colorectal cancer cell were compared to those of cells treated with antisense or nonsense Au-nanobeacons (Figure 6A, antisense Au-nanobeacon or nonsense Au-nanobeacon, respectively). No significant differences were found between cells treated with Au-nanobeacons and controls. Only one protein alpha-enolase displayed a higher level of expression (threefold) in both conditions (Figure 6A, Supplementary Figure S4-D-E and Table S1). The antisense Au-nanobeacon was responsible for triggering a sevenfold over-expression of the 40S ribosomal protein SA and the heat-shock protein 90-beta relative to the nonsense Au-nanobeacon (Figure 6A, Supplementary Figure S4-D-E and Table S1).

Discussion

To evaluate the full potential of the antisense Au-nanobeacon as nanotheranostics tool, we first discuss the capability of gene silencing via blockage of translation by conducting EGFP knockdown studies in HCT-116 cells using an EGFP expression plasmid as a target model, followed by a characterisation of the system effects in terms of cell viability, metabolic stress and DNA damage (genotoxicity). Additionally, a proteome profiling, for the same experimental conditions as those of EGFP silencing, is presented so as to identify putative protein markers of toxicity on HCT-116 cells.

EGFP fluorescence intensity as a direct indicator of EGFP silencing showed that only the antisense Au-nanobeacon at 30 nM effectively down-regulates EGFP expression (Figure 2). EGFP expression is not affected by either the nonsense Au-nanobeacon or nonsense oligonucleotide indicating that the knockdown is sequence specific. Interestingly, EGFP-targeting using the naked antisense oligonucleotide delivered with or without Lipofectamine did not result in EGFP silencing (Figure 2A). Confocal fluorescence imaging allowed for intracellular localisation pattern of the antisense Au-nanobeacons and direct evaluation of EGFP silencing associated with an increased Au-nanobeacon fluorescence that can be used to assess the silencing effect (Figure 3A). It should be emphasised that Au-nanobeacons require no transfection agent to enter cells. These results show that effective and specific gene silencing can be attained by

means of the proposed antisense Au-nanobeacons. The specificity and level of silencing can be directly correlated to the nanobeacon's fluorescence emission, which demonstrates the possibility of using this nanovectorisation approach as a nanotheranostics tool.

The future use of this system for *in vivo* models, and for clinical applications, clearly depends on the evaluation of its effects in the living system, i.e. toxicity evaluation. Therefore, we characterised the effects in terms of cell viability and metabolic stress, DNA damage (genotoxicity) and profiled the proteome response to the developed gene-silencing vehicle. In the present study HCT-116 was used as model but one should be aware that differences between cell lines do exist and that toxicity may depend on cell types. Moreover, toxicity may be a function of transfection efficiency, which would show a significant cell type-to-cell type variation, and therefore extrapolation to other systems is not straightforward. No cell viability changes and no major changes in GST activity were detected up to 48 h incubation, suggesting that no oxidative status changes occur within the cell following nanobeacon internalisation. These results are supported by the evidence that GST is inducible and its expression is directly modulated by the presence of oxidative radicals that inactivate the Keap repressor, which in turn releases the Nrf2 transcription factor of GST and other antioxidant enzymes (Kobayashi & Yamamoto 2005). The Au-nanobeacon approach may not elicit extensive oxidative damage, contrarily to what has been previously reported on internalisation of AuNPs and subsequent intracellular GSH depletion, promoting oxidative stress in HL7702 cells and lung fibroblasts (Li et al. 2010; Gao et al. 2011). The low oxidative stress induced by our approach, and hence low DNA damage, is in agreement with the genotoxicity assessment, in particular by the comet assay (see below).

In what comet assay is concerned, cells treated with antisense (39.66 ± 3.84%) and nonsense (32.28 ± 5.13%) Au-nanobeacons presented no significant differences to that of controls ($p < 0.05$). The uniform nucleoid distribution per class occurring amongst these samples (Figure 5B) has been previously reported in cultured cell lines not subjected to DNA-damage-inducing agents (Costa et al. 2012). These data show that the proposed antisense Au-nanobeacon strategy for gene silencing does not appear to significantly exhibit genotoxicity, which is in accordance with the expected reduced formation of oxidative radicals, generally regarded as a major cause of direct DNA strand breakage. Regarding samples treated with Lipofectamine (alone, and with both nonsense and antisense oligonucleotides), despite the verified differences in % of DNA in tail and class distribution (Figure 5B), Lipofectamine alone does not differ significantly from the control experiment. It has been previously shown that these cationic liposome-mediated transfection systems present toxic effects at concentrations higher than those used in this study and that liposome:DNA ratio modulates physicochemical properties of this complex and cytotoxic consequences upon its internalisation (Sakurai et al. 2000). Comparing antisense with nonsense oligonucleotide treatments (Figure 5C), no significant differences were found between Au-nanobeacons or Lipofectamine use for internalisation. DNA tail percentages above 80%, indicating extensive DNA damage and necrotic, apoptotic or nearly apoptotic cells (Choucroun et al. 2001; Hao et al. 2010), have not been observed with our approach, suggesting that, despite the observed variations, no severe genotoxic consequences arise from Au-nanobeacon internalisation. The rather elevated DNA % in tail value observed for cells expressing EGFP (46.58 ± 10.36%) might be associated with high mitotic activity of this cell line or to EGFP expression as previously reported (Liu et al. 1999; Chalfie & Kain 2006).

NAs usually arise due to errors during mitosis, essentially consisting of chromosomal aberrations deriving from incorrect segregation, and may translate into different observable abnormalities, such as micronuclei (Fenech et al. 2003). Our data showed no significant differences ($p < 0.05$) between control cells (expressing EGFP, and treated with AuNP@PEG) and cells transfected with either antisense or nonsense Au-nanobeacons. Thus far, such comprehensive evaluation of potential cyto- and/or genotoxic effects to the cell derived from AuNP-based vectorisation of gene-silencing strategies has never been presented. Here, effective gene regulation is attained without significant biological consequences, i.e. no decrease in cell viability, no perceptible oxidative stress and no increase of NA frequency and DNA strand breaks support the idea that the presented methodology bears no critical genotoxic or mutagenic consequences to the cell.

Regarding the proteome profiling, the effect of Lipofectamine as a transfection vehicle versus AuNPs as vectors for gene silencing in HCT-116 cells was firstly evaluated. We highlight the over-expression of protein 40S ribosomal protein SA that is required for the assembly and/or stability of the 40S ribosomal subunit and also functions as a cell surface receptor for laminin, playing a role in cell adhesion to the basal membrane (Venticinque & Meruelo 2012). Moreover, 19 additional proteins with less than 2-fold over-expression were identified in the presence of Lipofectamine, most of them acting as molecular chaperones that assist protein folding. These results indicate that Lipofectamine and AuNPs may induce a slight alteration of protein biosynthesis and folding, and induce cytoskeletal remodelling. Nevertheless, no relevant cellular toxicity is observed, which is in clear agreement with the data from cell viability, absence of oxidative stress and the lack of DNA strand breaks and NAs (see previous sections). Tedesco and co-workers showed similar effects by exposing *Mytilus edulis* to approximately 15 nm AuNPs (same size of our AuNPs), which lead to a small decrease in the levels of thiol proteins that they attributed to light oxidation (Tedesco et al. 2010). However, in our proteomic study we were not able to observe the reduction of thiol-containing proteins (Figure 6A and Supplementary Table S1). Interestingly, these authors were also not able to find lipid peroxidation (as indicator of oxidative damage) or induction of thioredoxin reductase activity (Tedesco et al. 2010). Despite no differences in protein expression levels in EGFP-transfected colorectal cancer cell to those of cells treated with antisense or nonsense Au-nanobeacons, the antisense Au-nanobeacon caused a sevenfold over-expression of the 40S ribosomal protein SA

and the heat-shock protein 90-beta relative to the Nonsense Au-nanobeacon (Figure 6A, Supplementary Figure S4-D-E and Table S1). These over-expression values may result from an alteration of cell homeostasis related with EGFP production, as EGFP silencing by antisense Au-nanobeacon may trigger mechanisms of cellular stress response. In support of this idea, we can observe an increase in the expression levels of cellular chaperones, namely heat-shock proteins encoded by HSP90B, HSP71 and HSP7C genes, different T-complex subunits and calreticulin. Peptidyl-prolylcis-trans isomerase (a component of non-ligated steroid receptors heterocomplexes through interaction with heat-shock protein 90 that may play a role in the intracellular trafficking of hetero-oligomeric forms of steroid hormone receptors between cytoplasm and nuclear compartments) and peptide 35 (no protein identification) expression levels were reduced (1.5-fold) in the presence of antisense Au-nanobeacon relative to nonsense Au-nanobeacon and with similar expression levels in the other tested conditions (Figure 6A and B, Supplementary Figure S4-D-E and Table S1).

Conclusions

We developed a robust and versatile system with nanotheranostics potential capable of blocking specific gene expression via an antisense Au-nanobeacon. A significant attribute of these Au-nanobeacons is the ability to attain similar levels of inhibition of gene expression with lower amounts than those of free oligonucleotides. This extraordinary efficiency occurs probably due to the large payload capacity of the NPs. The nanobeacon conformation allows for detection of silencing events as it occurs inside cells; thus, our approach becomes simple, inexpensive and straightforward as adjustment to any specific target can be easily made.

Evaluating biocompatibility and safety issues of these nanomaterials is imperative towards its use for medical purposes. However, the vast majority of studies report only on the biocompatibility of nanomaterials through the study of cell viability. Here, we went one step further and provide for the first time an extensive toxicity study of NPs for gene therapy. Modulation of gene expression was successfully attained with 30 nM of antisense Au-nanobeacon, without decreased cell viability or induction of oxidative stress. Moreover, an assessment of genome-related toxicity revealed no significant DNA damage increase, as well as no potential mutagenic or clastogenic consequences to the cell. Proteomics appears to be a relevant approach for mechanistic studies of cellular responses to Au-nanobeacons. The proteome profiling, as presented here, represents a useful tool for systematic analysis of toxicity of nanoconjugates, not only at the molecular level but also for the discovery of biomarkers and pathways towards the understanding of the mechanisms of toxicity. It must be emphasised that such mechanistic studies must be ultimately verified on relevant *in vivo* models. Identification of response pathways to AuNP internalisation may assist in gathering relevant information on acute toxicity so as to optimise systems for translation to *in vivo* models, and eventually to clinical applications.

Acknowledgements

This work was funded by Fundação para a Ciência e Tecnologia, Ministry of Science and Education (FCT/MEC): CIGMH (PEst-OE/SAU/UI0009/2011); REQUIMTE (PEst-C/EQB/LA0006/2011); PTDC/QUI-QUI/112597/2009; PTDC/CTM-NAN/109877/2009; PTDC/BBB-NAN/1812/2012; J.C. for SFRH/BD/62957/2009; ML for SFRH/BD/64026/2009; PC for SFRH/BPD/72564/2010; LRR for SFRH/BD/70202/2010. Additional funding was from the Nanotruck-Action from NanoSciEra^{+}.

Declaration of interest

The authors declare that they have no competing interests.

References

Akhtar S, Benter IF. 2007. Nonviral delivery of synthetic siRNAs in vivo. J Clin Invest 117:3623–3632.

Alkilany AM, Murphy CJ. 2010. Toxicity and cellular uptake of gold nanoparticles: what we have learned so far? J Nanopart Res 12:2313–2333.

Chalfie M, Kain SR. 2006. Green fluorescent protein: properties, applications and protocols. New Jersey, USA: Wiley and Sons, Inc.

Choucroun P, Gillet D, Dorange G, Sawicki B, Dewitte JD. 2001. Comet assay and early apoptosis. Mutat Res 478:89–96.

Conde J, Ambrosone A, Sanz V, Hernandez Y, Marchesano V, Tian F, et al. 2012a. Design of multifunctional gold nanoparticles for in vitro and in vivo gene silencing. ACS Nano 6:8316–8324.

Conde J, de la Fuente JM, Baptista PV. 2010. In vitro transcription and translation inhibition via DNA functionalized gold nanoparticles. Nanotechnology 21:505101.

Conde J, Doria G, Baptista P. 2012b. Noble metal nanoparticles applications in cancer. J Drug Deliv 2012:751075.

Conde J, Rosa J, de la Fuente JM, Baptista PV. 2013. Gold-Nanobeacons for simultaneous gene specific silencing and intracellular tracking of the silencing events Biomaterials. 34:2516–2523.

Costa PM, Costa MH. 2007. Genotoxicity assessment in fish peripheral blood: a method for a more efficient analysis of micronuclei. J Fish Biol 71:148–151.

Costa PM, Lobo J, Caeiro S, Martins M, Ferreira AM, Caetano M, et al. 2008. Genotoxic damage in Soleasenegalensis exposed to sediments from the Sado Estuary (Portugal): effects of metallic and organic contaminants. Mutat Res 654:29–37.

Costa PM, Milhinhos A, Simões M, Marum L, Oliveira AM, Costa MH, et al. 2012. Determining DNA strand breakage from embryogenic cell cultures of a conifer species using the single-cell gel electrophoresis assay. Tree Genet Genomes 8:425–430.

Daniel MC, Astruc D. 2004. Gold nanoparticles: assembly, supramolecular chemistry, quantum-size-related properties, and applications toward biology, catalysis, and nanotechnology. Chem Rev 104:293–346.

Dobrovolskaia MA, McNeil SE. 2007. Immunological properties of engineered nanomaterials. Nat Nanotechnol 2:469–478.

Doria G, Conde J, Veigas B, Giestas L, Almeida C, Assunção M, et al. 2012. Noble metal nanoparticles for biosensing applications. Sensors (Basel) 12:1657–1687.

Fenech M, Chang WP, Kirsch-Volders M, Holland N, Bonassi S, Zeiger E. 2003. HUMN project: detailed description of the scoring criteria for the cytokinesis-block micronucleus assay using isolated human lymphocyte cultures. Mutat Res 534:65–75.

Gao W, Xu K, Ji L, Tang B. 2011. Effect of gold nanoparticles on glutathione depletion-induced hydrogen peroxide generation and apoptosis in HL7702 cells. Toxicol Lett 205:86–95.

Ghosh P, Han G, De M, Kim CK, Rotello VM. 2008a. Gold nanoparticles in delivery applications. Adv Drug Deliv Rev 60:1307–1315.

Ghosh PS, Kim CK, Han G, Forbes NS, Rotello VM. 2008b. Efficient gene delivery vectors by tuning the surface charge density of amino acid-functionalized gold nanoparticles. ACS Nano 2:2213–2218.

Giljohann DA, Seferos DS, Prigodich AE, Patel PC, Mirkin CA. 2009. Gene regulation with polyvalent siRNA-nanoparticle conjugates. J Am Chem Soc 131:2072–2073.

Habig WH, Pabst MJ, Jakoby WB. 1974. Glutathione S-transferases. The first enzymatic step in mercapturic acid formation. J Biol Chem 249:7130–7139.
Haglund E, Seale-Goldsmith MM, Leary JF. 2009. Design of multifunctional nanomedical systems. Ann Biomed Eng 37:2048–2063.
Hao H, Lei F, Nancai Y, Wen S, Xiaojuan Q. 2010. The single-cell gel electrophoresis assay to determine apoptosis induced by siRNA in Colo 320 cells. Afr J Biotechnol 8:3731–3733.
Jain KK. 2008. Nanomedicine: application of nanobiotechnology in medical practice. Med Princ Pract 17:89–101.
Kim SS, Garg H, Joshi A, Manjunath N. 2009. Strategies for targeted nonviral delivery of siRNAs in vivo. Trends Mol Med 15:491–500.
Kobayashi M, Yamamoto M. 2005. Molecular mechanisms activating the Nrf2–Keap1 pathway of antioxidant gene regulation. Antioxid Redox Signal 7:385–394.
Lee PC, Meisel D. 1982. Adsorption and surface-enhanced Raman of dyes on silver and gold sols. J Phys Chem 86:3391–3395.
Li JJ, Hartono D, Ong CN, Bay BH, Yung LY. 2010. Autophagy and oxidative stress associated with gold nanoparticles. Biomaterials 31:5996–6003.
Liu HS, Jan MS, Chou CK, Chen PH, Ke NJ. 1999. Is green fluorescent protein toxic to the living cells? Biochem. Biophys Res Commun 260:712–717.
Liu Y, Shipton MK, Ryan J, Kaufman ED, Franzen S, Feldheim DL. 2007. Synthesis, stability, and cellular internalization of gold nanoparticles containing mixed peptide-poly(ethylene glycol) monolayers. Anal Chem 79:2221–2229.
Livak KJ, Schmittgen TD. 2001. Analysis of relative gene expression data using real-time quantitative PCR and the 2(-Delta DeltaC(T)) method. Methods 25:402–408.
McIntosh CM, Esposito EA, III Boal AK, Simard JM, Martin CT, Rotello VM. 2001. Inhibition of DNA transcription using cationic mixed monolayer protected gold clusters. J Am Chem Soc 123:7626–7629.
Ozpolat B, Sood AK, Lopez-Berestein G. 2010. Nanomedicine based approaches for the delivery of siRNA in cancer. J Intern Med 267:44–53.
Pfaffl MW. 2001. A new mathematical model for relative quantification in real-time RT-PCR. Nucleic Acids Res 29:e45.
Rana S, Bajaj A, Mout R, Rotello VM. 2012. Monolayer coated gold nanoparticles for delivery applications. Adv Drug Deliv Rev 64:200–216.
Rosa J, Conde J, de la Fuente JM, Lima JC, Baptista PV. 2012. Gold-nanobeacons for real-time monitoring of RNA synthesis. Biosens Bioelectron 36:161–167.
Rosi NL, Giljohann DA, Thaxton CS, Lytton-Jean AK, Han MS, Mirkin CA. 2006. Oligonucleotide-modified gold nanoparticles for intracellular gene regulation. Science 312:1027–1030.
Sakurai F, Inoue R, Nishino Y, Okuda A, Matsumoto O, Taga T, et al. 2000. Effect of DNA/liposome mixing ratio on the physicochemical characteristics, cellular uptake and intracellular trafficking of plasmid DNA/cationic liposome complexes and subsequent gene expression. J Control Release 66:255–269.
Sanz V, Conde J, Hernandez Y, Baptista PV, Ibarra MR, de la Fuente JM. 2012. Effect of PEG biofunctional spacers and TAT peptide on dsRNA loading on gold nanoparticles. J Nanopart Res 14:1–9.
Singh NP, McCoy MT, Tice RR, Schneider EL. 1988. A simple technique for quantitation of low levels of DNA damage in individual cells. Exp Cell Res 175:184–191.
Tedesco S, Doyle H, Blasco J, Redmond G, Sheehan D. 2010. Exposure of the blue mussel, Mytilus edulis, to gold nanoparticles and the pro-oxidant menadione. Comp Biochem Physiol C Toxicol Pharmacol 151:167–174.
Teixeira MC, Santos PM, Fernandes AR, Sá-Correia I. 2005. A proteome analysis of the yeast response to the herbicide 2,4-dichlorophenoxyacetic acid. Proteomics 5:1889–1901.
Thomas M, Klibanov AM. 2003. Conjugation to gold nanoparticles enhances polyethylenimine's transfer of plasmid DNA into mammalian cells. Proc Natl Acad Sci USA 100:9138–9143.
van MJ, Kaspers GJ, Cloos J. 2011. Cell sensitivity assays: the MTT assay. Methods Mol Biol 731:237–245.
Venticinque L, Meruelo D. 2012. Comprehensive proteomic analysis of nonintegrin laminin receptor interacting proteins. J Proteome Res 11:4863–4872.
Wall NR, Shi Y. 2003. Small RNA: can RNA interference be exploited for therapy? Lancet 362:1401–1403.
Whitehead KA, Langer R, Anderson DG. 2009. Knocking down barriers: advances in siRNA delivery. Nat Rev Drug Discov 8:129–138.
Zhang XD, Wu D, Shen X, Liu PX, Yang N, Zhao B, et al. 2011. Size-dependent in vivo toxicity of PEG-coated gold nanoparticles. Int J Nanomedicine 6:2071–2081.

Supplementary materials available online

Supplementary Table S1
Supplementary Figures S1–S4